JMEPEG (2012) 21:2177–2187
DOI: 10.1007/s11665-012-0143-1

1059-9495/$19.00

Surface Modification and In Vitro Characterization of Cp-Ti and Ti-5Al-2Nb-1Ta Alloy in Simulated Body Fluid

Y. Sasikumar and N. Rajendran

(Submitted August 8, 2011; in revised form December 8, 2011)

Ti and its alloys are widely used in manufacturing orthopedic implants as prostheses for joint replacement because of their high corrosion resistance and excellent biocompatibility. However, they lack in bone-bonding ability and leads to higher rate of osteolysis and subsequent loosening of implants. In order to enhance the bone-bonding ability of these alloys, various surface-modification techniques are generally employed. The present investigation is mainly concerned with the surface modification of Cp-Ti and Ti-5Al-2Nb-1Ta alloy using a mixture of alkali and hydrogen peroxide followed by subsequent heat treatment to produce a porous gel layer with anatase structure, which enhances osseointegration. The morphological behavior was examined by x-ray diffractometer (XRD), atomic force microscopy (AFM), and scanning electron microscopy (SEM) coupled with energy dispersive x-ray analysis (EDX). The in vitro characterization of all the specimens was evaluated by immersing the specimens in simulated body fluid solution to assess the apatite formation over the metal surface. The apatite formation was confirmed by XRD, SEM-EDX, and Fourier transform infrared spectroscopy (FT-IR). Further, the electrochemical corrosion behaviors of both the untreated and treated specimens were evaluated using potentiodynamic polarization and electrochemical impedance spectroscopy. The results revealed that the surface-modified and heat-treated specimens exhibited higher corrosion resistance and excellent biocompatibility when compared to the chemical and untreated specimens.

Keywords AFM, apatite, biomaterial, polarization, simulated body fluid, Ti alloy

1. Introduction

Ti and its alloys are used in orthopedic applications owing to their favorable mechanical properties, good biocompatibility, and their excellent corrosion resistance (Ref 1, 2). Ti-6Al-4V alloy with ($\alpha + \beta$) structure was the first Ti alloy used as implant material. It was widely used for orthopedic implants and was found that V and Al were released into the cell tissue by way of passive film dissolution (Ref 3) and wear process (Ref 4, 5). Moreover, V is classified in the toxic group (Ref 6). Hence, it becomes necessary to select non-toxic metals as alloying elements for biomedical applications. Hence, vanadium-free Ti alloys like Ti-6Al-7Nb are widely used as an alternative to Ti-6Al-4V, where V is replaced by Nb which is also a β-phase stabilizer. One percent of Ta is also added to the above alloy to enhance the corrosion resistance, and hence, the alloy becomes Ti-5Al-2Nb-1Ta. Research studies also reveal that Ta, Nb, Zr, and Mo are non-toxic and long-term biocompatible (Ref 7-9). Besides, they are expected to improve mechanical properties and corrosion resistance.

Y. Sasikumar and **N. Rajendran**, Department of Chemistry, Anna University, Chennai 600 025, India. Contact e-mail: nrajendran@annauniv.edu.

To improve the wear resistance of Ti and its alloys, they are subjected to various surface treatments, such as thermal spraying, plasma vapor deposition processes, anodic oxidation, ion implantation, glow discharge nitriding, and laser treatment (Ref 10-12). The method of inducing bioactivity in the implant by chemical surface modification was reported by Ohtsuki et al. (Ref 13). Wen et al. (Ref 14) evaluated the bioactivity of Ti alloy by two-step chemical treatment using the combination of acids ($HCl + H_2SO_4$) followed by alkali treatment. Kokubo et al. (Ref 15) introduced alkali and the subsequent heat treatment as a method of surface modification for Ti alloys to improve the bioactivity. Sasikumar et al. (Ref 16) evaluated the bioactivity of Ti-15Mo alloy by alkali treatment followed by heat treatment.

Thus, numerous reports are available on the alkali-treated and hydrogen peroxide-treated Ti alloys and their electrochemical studies (Ref 17-20). However, the reports pertaining to the corrosion behavior of surface-modified Ti alloys by the combination of alkali and hydrogen peroxide are still scarce.

Hence, the objective of the present investigation is mainly concerned with the surface modification of Cp-Ti and Ti-5Al-2Nb-1Ta alloy using mixture of alkali and hydrogen peroxide followed by heat treatment to improve the bioactivity of the material. The in vitro bioactivity of surface-modified specimens was analyzed by immersing them in simulated body fluid (SBF) solution. The formation of the apatite layer was confirmed by x-ray diffractometer (XRD), Fourier transform infrared (FT-IR) spectroscopy and scanning electron microscopy (SEM). Further, the corrosion behavior of the specimens was characterized using potentiodynamic polarization and electrochemical impedance spectroscopy (EIS).

2. Materials and Methods

2.1 Specimen Preparation

The Cp-Ti and Ti-5Al-2Nb-1Ta alloy (Kobe Steel Ltd., Japan) specimens with surface area of 1 cm^2 and with chemical composition presented in Table 1 were used for this study. The specimens were polished using abrasive SiC paper up to 1200 grade. Final polishing was done using alumina powder (0.5 μm in powder size) to produce a mirror-finish surface followed by rinsing with distilled water and cleaned with acetone followed by ultrasonication for 20 min. Finally, the specimens were washed in distilled water and dried in an oven.

2.2 Surface Treatment

The specimens were immersed in 20 mL of aqueous solution containing molar concentrations (M) of 10 M NaOH and 4.5 M H_2O_2 solution kept at 60 °C in an oven for 1 h, gently washed with distilled water, and then dried at 40 °C. Then, the specimens were subsequently heat treated in an electric furnace (induction type) at temperature of 600 °C for 1 h in an air atmosphere and then allowed to cool to room temperature. Finally, the specimens were ultrasonically cleaned to remove the loosely attached particles over the surface of the specimens.

2.3 Surface Characterization

X-ray diffraction patterns were recorded with Bruker D8 diffractometer using Cu-Kα radiation at a scan rate of (2θ) 0.02°. The scanning range was from 20° to 50°. The surface topography of the modified specimens was recorded using atomic force microscopy (AFM), Seiko Instruments (SII), Japan. The images were acquired by non-contact mode using Au-coated silicon cantilevers with a spring constant of 1.6 N/m at a resonant frequency of 26 kHz. All the images were recorded under normal atmospheric conditions. The surface morphology of the specimens was examined using SEM on a Hitachi model S-4800. FT-IR characterization of the specimens was recorded in the range of 400-4000 cm^{-1} on a Perkin-Elmer using the KBr technique to confirm the existence of phosphate and carbonate groups.

2.4 Electrochemical Characterization

Electrochemical experiments were performed using a conventional three-electrode cell assembly maintained at 37 °C. A saturated Ag/AgCl electrode served as a reference electrode, platinum sheet acted as a counter electrode, and the test material as the working electrode. The SBF solution was used as the electrolyte, and the SBF solution was prepared, and the in vitro experiments were carried out using a previously reported procedure (Ref 21). The composition of the SBF solution is presented in Table 2.

Corrosion measurements for the specimens were conducted in SBF solution using a potentiostat model (PGSTAT 12, AUTOLAB, The Netherlands B.V.) which was controlled by a personal computer. Potentiodynamic polarization studies were carried out at a scan rate of 0.001 V/s using dedicated software. In order to obtain reliable results, polarization experiments were triplicated in SBF solution. EIS measurements were performed with a frequency ranging from 10^{-2} to 10^4 Hz using an electrochemical system frequency response analyzer (FRA). The amplitude of the superimposed A.C. signal was 10 mV peak-to-peak voltage. The data obtained in terms of impedance spectra (Bode plots) were interpreted and fitted using a nonlinear least square (NLLS) method.

3. Results and Discussion

3.1 Morphological Characterization

The XRD patterns for untreated (UT), alkali hydrogen peroxide-treated (AHT) and alkali hydrogen peroxide heat-treated (AHHT) Ti specimens are shown in Fig. 1(a). The UT Ti pattern showed the Ti peaks at 2θ values of 35°, 38°, and 40° corresponding to the planes of (100), (002), and (101), respectively. The AHT Ti pattern showed the intense diffraction peaks at 2θ values of 23.5° and 27°, which represent the formation of sodium titanate over the metal surface. The AHHT Ti pattern showed the intense diffraction peaks at 2θ values of 23.5°, 27°, and 27.5°, which represent the formation of prism sodium titanate due to the subsequent heat treatment. The AHT and AHHT Ti patterns exhibited the diffraction peak at 2θ value of 28.5° corresponding to the plane (210), which represents the characteristic peak of the anatase phase of Ti dioxide present on the surface of the specimens. It has been reported that the prism sodium titanate possess high crystallinity because of the subsequent heat treatment over the alkali and heat-treated Ti alloys (Ref 22).

The XRD patterns for UT, AHT, and AHHT Ti-5Al-2Nb-1Ta alloys are shown in Fig. 1(b). The UT Ti-5Al-2Nb-1Ta

Table 2 Chemical composition of SBF solution

S. No.	Reagents used	Grams in 1000 mL
1	NaCl	8.03
2	$NaHCO_3$	0.35
3	KCl	0.22
4	$K_2HPO_4{\cdot}3H_2O$	0.23
5	$MgCl_2{\cdot}6H_2O$	0.31
6	$CaCl_2$	0.29
7	Na_2SO_4	0.07
8	$((HOCH_2)_3CNH_2)$	6.11
9	1 M HCl	1-4 mL

Table 1 Chemical compositions of Ti and Ti-5Al-2Nb-1Ta alloy in wt.%

	Main alloying elements, wt.%									
Alloy	C	N	O	H	Ta	Fe	Mo	Al	Nb	Ti
Ti	0.002	0.01	0.14	0.001	0.005	0.03	0.02	0.008	…	Bal.
Ti-5Al-2Nb-1Ta	0.05	0.004	0.17	0.001	0.95	0.21	0.77	5.90	1.98	Bal.

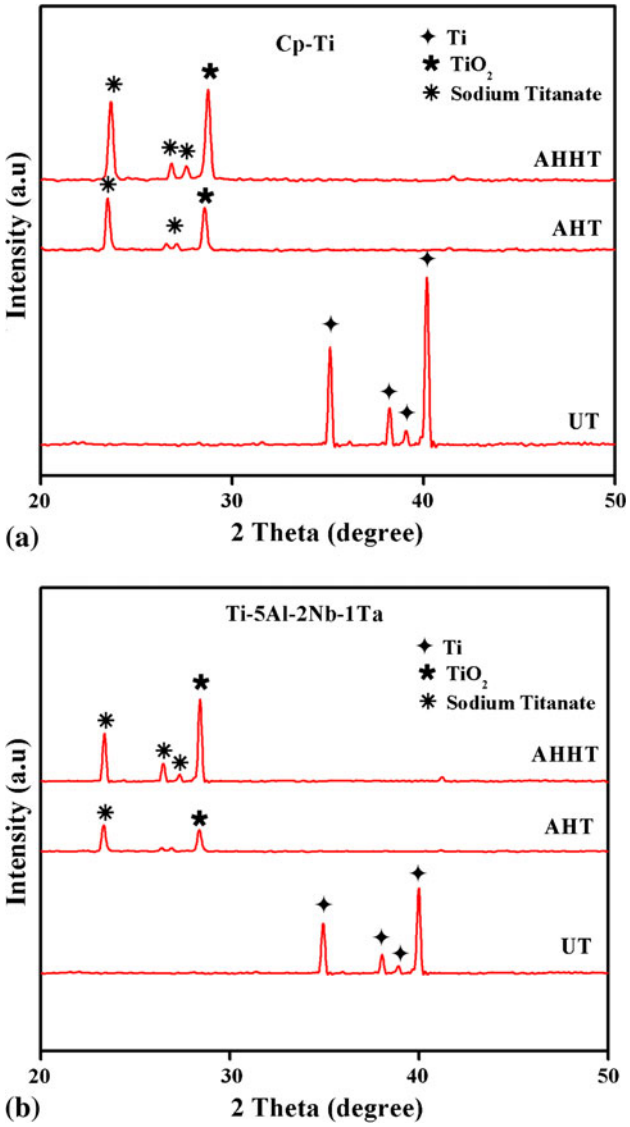

Fig. 1 XRD patterns of (a) Ti and (b) Ti-5Al-2Nb-1Ta alloy

alloy showed the diffraction pattern of Ti peaks at 2θ values of 35°, 38° and 40° corresponding to the planes of (120), (111) and (200), respectively. The AHT Ti-5Al-2Nb-1Ta alloy showed the diffraction pattern at 2θ value of 23.3°, which represents the formation of sodium titanate over the surface-modified Ti-5Al-2Nb-1Ta alloy. The AHHT Ti-5Al-2Nb-1Ta alloy showed the diffraction pattern at 2θ values of 23.3°, 26.5° and 27.3°, which represent the prism sodium titanate formation due to the subsequent heat treatment. The diffraction peak at 2θ value of 28.5° corresponding to the plane (210) represents the characteristic peak of the anatase phase of Ti dioxide present on the surface of the AHT and AHHT Ti-5Al-2Nb-1Ta specimens.

The AFM images of UT, AHT, and AHHT Ti and Ti-5Al-2Nb-1Ta specimens are shown in Fig. 2(a)-(f). The three-dimensional topographic images of UT Ti and Ti-5Al-2Nb-1Ta alloy reveal smooth, uniform surfaces. The AHT Ti and Ti-5Al-2Nb-1Ta alloy showed a porous network structure, whereas the porous network structure arranged with a preferred orientation was observed for AHHT Ti-5Al-2Nb-1Ta alloy (Ref 23). After the thermal treatment, the thicknesses of the AHHT Ti and Ti-5Al-2Nb-1Ta alloy were found to be reduced. This reduction phenomenon is attributed because of the agglomerations formed (as evinced from the SEM images) during the thermal treatment.

The SEM micrographs of UT, AHT, and AHHT Ti and Ti-5Al-2Nb-1Ta alloy are depicted in Fig. 3(a)-(f). The UT Ti and Ti-5Al-2Nb-1Ta revealed dense and relatively smooth uniform surfaces with oriental grooves, which represent the typical morphology of the mechanically polished surface. The AHT Ti showed a fine trabecular with uniform porous network structure. The pore diameter was found to be varying from micrometer to nanometer scale, and this porous network morphology depends upon the concentration of mixture of alkali and hydrogen peroxide and the condition of the treatment (Ref 24). On the other hand, the AHT Ti-5Al-2Nb-1Ta alloy showed non-homogenous surface with a number of crests and troughs. The occurrence of crests and troughs on the specimen indicated that the oxide layer on the surface does not grow uniformly, which may be due to the surface imperfections during the chemical treatment. The AHHT Ti revealed a rod-like structure with a cracked morphology, which may be due to the dehydration process during the heat treatment, and a thick oxide layer was observed, and revealed the formation of prism sodium titanate over the surface-modified Ti specimens whereas, the AHHT Ti-5Al-2Nb-1Ta alloy showed an agglomerated surface with non-homogeneity in nature. This agglomerated morphology indicated that the alloying elements of Nb and Ta particles get mixed up with the sodium ions and adsorbed over the entire surface of the specimen during the process of heat treatment. The adsorbed agglomerated surface represents the formation of sodium titanate as confirmed from the XRD analysis.

3.2 In Vitro Characterization

In order to assess the biocompatibility of the material, the UT, AHT, and AHHT Ti and Ti-5Al-2Nb-1Ta alloy were immersed in SBF solution for 7 days. The XRD patterns for UT, AHT, and AHHT Ti and Ti-5Al-2Nb-1Ta alloy after 7 days of immersion in SBF solution are shown in Fig. 4(a) and (b). After the immersion in SBF solution, the crystalline sodium titanate has been transformed into apatite peaks at 2θ values of 26.7° and 49.5° corresponding to the planes of (002) and (102), respectively, for the UT Ti and AHHT Ti-5Al-2Nb-1Ta alloy. The distinctive sharp peaks at 26.7° and 32° correspond to the planes of (002) and (211), respectively, ascribed to the formation of crystalline apatite for the AHHT Ti and AHT Ti and Ti-5Al-2Nb-1Ta specimens. The formation of the crystalline apatite over the AHT and AHHT specimens indicated that the network structure formed on the surface of Ti could induce the nucleation and growth of bone-like apatite on its surface (Ref 22). However, none of the specimens showed any peaks corresponding to Ti after the immersion in SBF solution, thus indicating the thick apatite layer formation over the surface of the specimens. The UT Ti-5Al-2Nb-1Ta alloy showed no diffraction peaks, indicating the absence of apatite formation over the surface of the specimen.

The average crystallite size of surface-modified Ti and Ti-5Al-2Nb-1Ta alloys was calculated using Scherer's equation (Ref 25) as follows:

$$D_{hkl} = k\lambda/[B\cos\theta] \quad \text{(Eq 1)}$$

where B is the difference in the width of the half-maximum of the peaks of the pure diffraction profile in radians, k is a

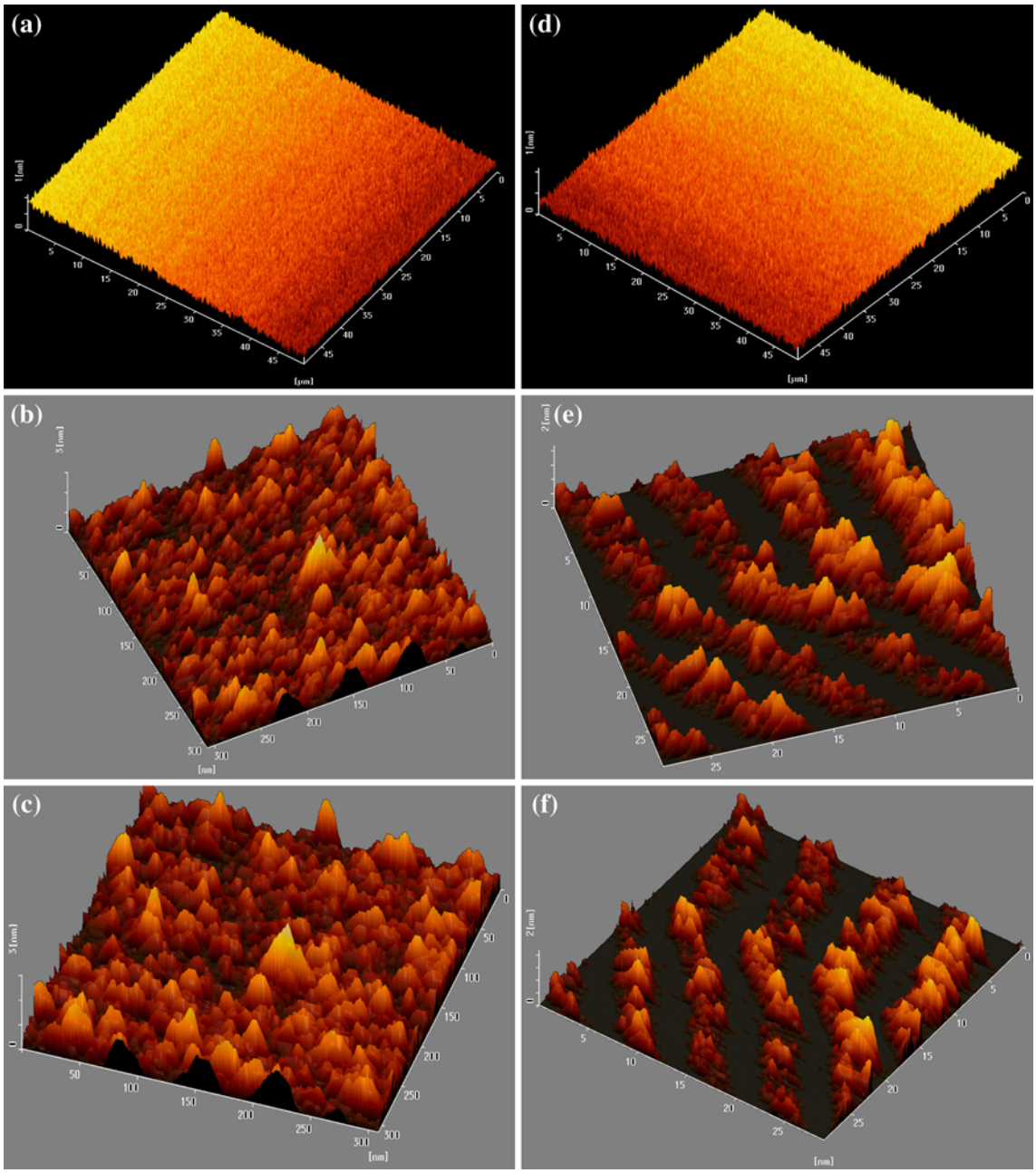

Fig. 2 AFM topographic images of Ti: (a) UT, (b) AHT, (c) AHHT, and Ti-5Al-2Nb-1Ta alloy: (d) UT, (e) AHT, and (f) AHHT

constant (shape factor 0.89), λ is the wavelength of the x-rays (0.154056 nm), θ is the diffraction angle, and D_{hkl} is the average diameter of the crystallite. From the estimated data, the calculated average crystallite sizes are found in the range of 30-50 nm.

In the implant applications, the bone plates for internal fixation, is one of the main key requirements for the successful osseointegration, i.e., the bone bioactivity, is determined by the apatite forming ability of the implant surface in body fluids. In vitro evaluation of apatite-forming ability is commonly carried out using immersion test in SBF solution for a soaking period of the order of few weeks (Ref 26).

The bioactivity of a material is associated with its ability to form an apatite layer when implanted or kept in contact with a biological fluid (Ref 27). FT-IR analysis was carried out to confirm the formation of apatite particles over the surface of the specimens on immersion in SBF solution. The FT-IR spectra of UT, AHT, and AHHT Ti and AHT and AHHT Ti-5Al-2Nb-1Ta alloy after 7 days of immersion in SBF solution are presented in Fig. 5(a) and (b).

A broad absorption band at 3440-3600 cm^{-1} and the bending modes at 1639 and 1630 cm^{-1} revealed the O-H stretching and bending vibrations of adsorbed H_2O. The presence of PO_4^{3-} group is also ascertained from the peaks observed at 597, 1032, and 1037 cm^{-1}. The peak corresponding to P-OH stretching was observed at 910 cm^{-1}, while CO_3^{2-} peaks were observed at 1467 and 1400 cm^{-1} (Ref 28). The triply (v_4) and doubly (v_2) degenerated bending modes of phosphate's O-P-O bonds were found at 602, 562, and 597 cm^{-1} (Ref 29). The bands detected at 875 cm^{-1} were

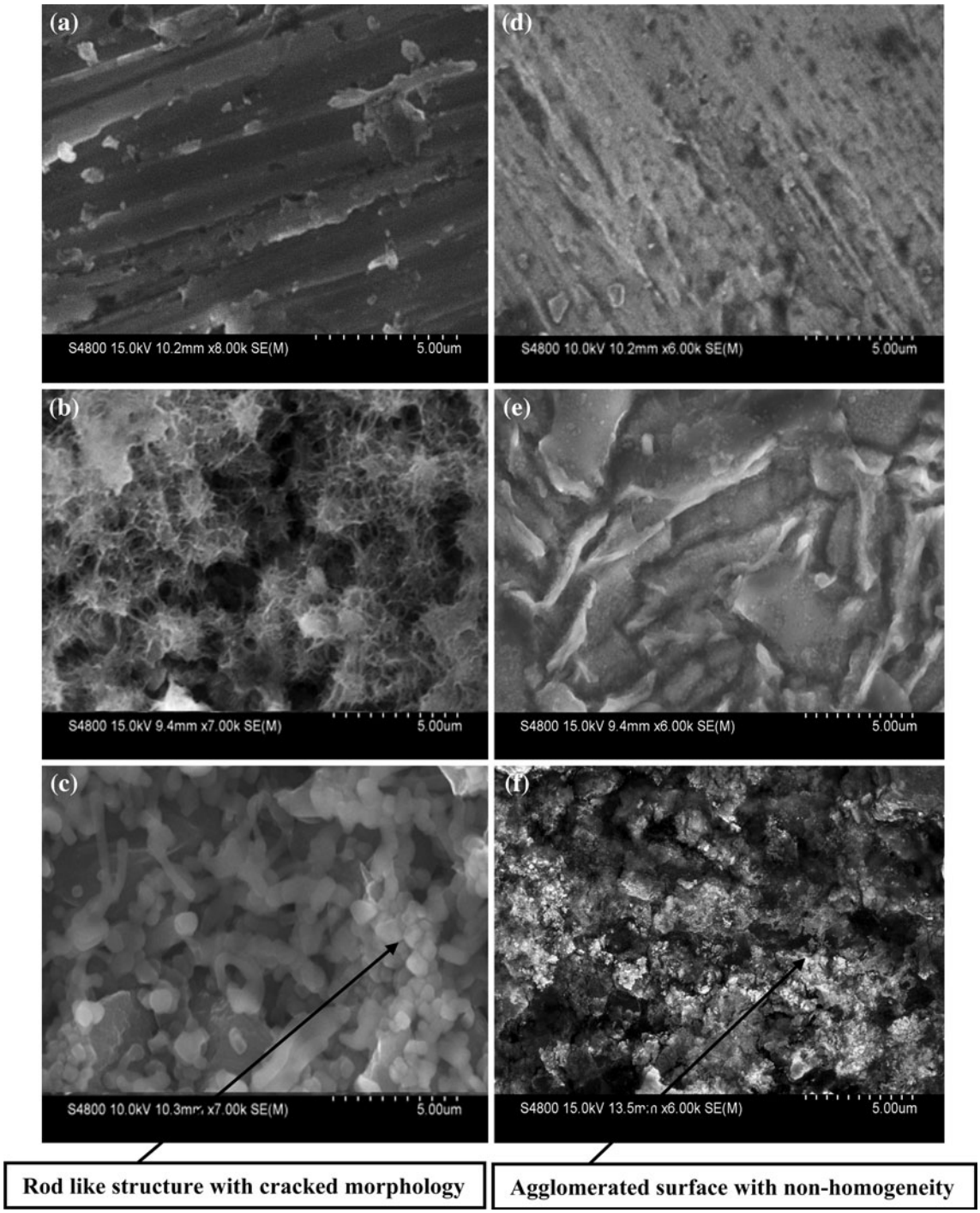

Fig. 3 SEM micrographs of Ti: (a) UT, (b) AHT, (c) AHHT, and Ti-5Al-2Nb-1Ta: (d) UT, (e) AHT, and (f) AHHT

assigned to the CO_3^{2-} group of B-type carbonated apatite, where PO_4^{3-} groups are substituted by CO_3^{2-}. The peaks corresponding to phosphate and carbonate functional groups could be identified on the spectra which confirm the formation of apatite layer. Similar results were reported for the FT-IR analysis of apatite (Ref 30-32). Hence, the appearance of the phosphate and carbonate absorption bands in the spectra of the UT, AHT and AHHT Ti and Ti-5Al-2Nb-1Ta alloy after soaking in SBF solution confirmed the formation of an apatite layer. Once the apatite nuclei are formed, they grow spontaneously by consuming the calcium and phosphate ions from the SBF solution, as the solution is supersaturated with respect to the apatite (Ref 33, 34). The above observation clearly reveals the growth layer which is essentially the carbonated incorporated apatite and the presence of apatite growth on the surface-modified specimens. However, the UT Ti-5Al-2Nb-1Ta showed no particles to characterize for FT-IR analysis, as no significant result is obtained for this specimen.

The SEM micrographs of UT, AHT, and AHHT Ti and Ti-5Al-2Nb-1Ta alloy immersed in SBF solution for 7 days are depicted in Fig. 6(a)-(f). After soaking in SBF solution, the morphology and composition of the UT, AHT, and AHHT

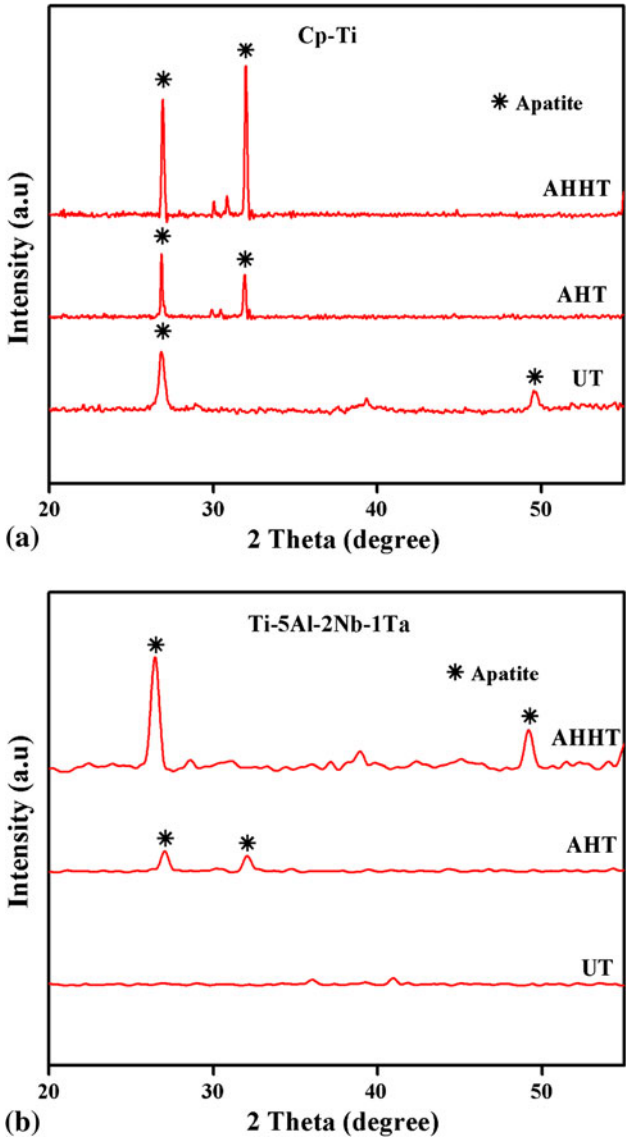

Fig. 4 XRD patterns of (a) Ti and (b) Ti-5Al-2Nb-1Ta alloy after 7 days of immersion in SBF solution

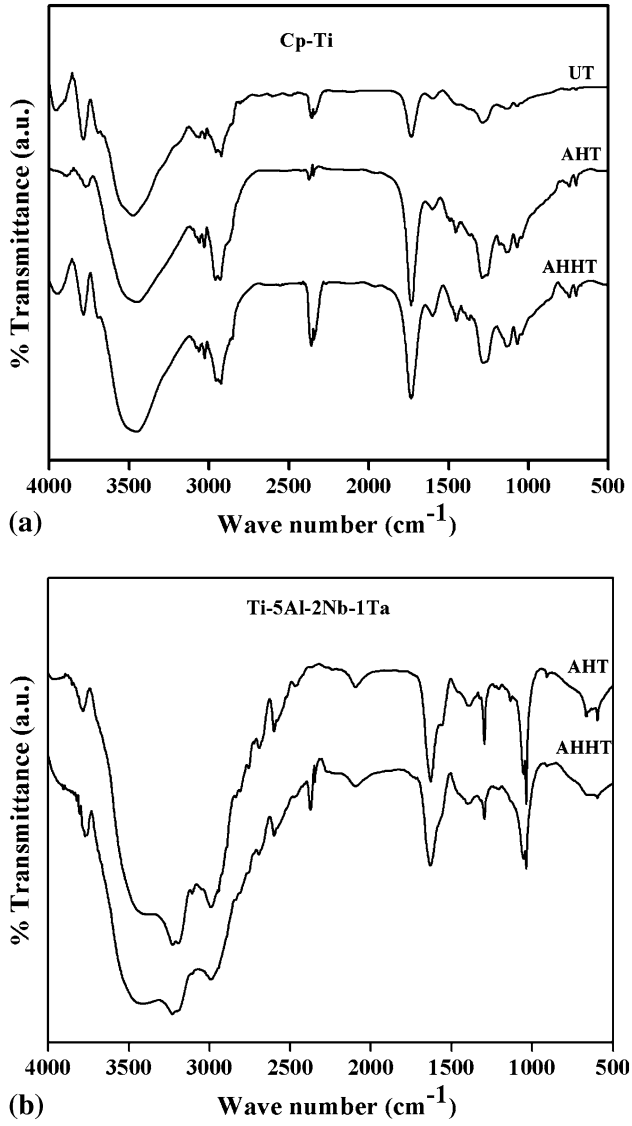

Fig. 5 FT-IR spectra of (a) Ti and (b) Ti-5Al-2Nb-1Ta alloy after 7 days of immersion in SBF solution

Ti-5Al-2Nb-1Ta specimens exhibited significant variation, confirming the materials ability to interact with the ions present in the SBF solution. It could be observed that the surface of UT Ti showed only a few white particles formed randomly over the surface, whereas the UT Ti-5Al-2Nb-1Ta alloy exhibited a smooth surface and showed no particles, indicating the absence of the apatite particles over the metal surface. The AHT Ti showed a cluster of ball-like apatite particles over the surface of the specimen, whereas the AHT Ti-5Al-2Nb-1Ta alloy exhibited a few apatite-like particles randomly scattered over the surface of the specimen. The AHHT Ti revealed an isolated globular in shape of apatite-like particles over the entire surface of the specimen which may be due to the prolonged interaction of calcium and phosphate ions adsorbed on the surface-modified Ti. On the other hand, the AHHT Ti-5Al-2Nb-1Ta alloy revealed a cluster of spherical apatite-like particles randomly on the porous sodium titanate layer, formed after the heat treatment (Ref 20).

The formation of the bioactive material could be induced by the presence of Ti-OH groups, which reveals negative charge to interact with calcium ions present in the SBF solution. The amorphous calcium titanate is postulated to reveal positive charge, thereby interacting with the phosphate ions in the fluid to form the amorphous calcium phosphate, which eventually crystallized into hydroxyapatite particles (Ref 14). Moreover, with the formation of apatite layer on the surface, the supersaturation of simulated physiological solution may promote preferential nucleation of apatite on the formed apatite than in the solution because of the higher activation energy for the homogenous nucleation of apatite in the human body fluid.

3.3 Electrochemical Characterization

The electrochemical characterization was performed to evaluate the protective effectiveness of the surface layers formed on the specimens during chemical and heat treatment. The surface treatments also have profound effect on the electrochemical behavior during the immersion in SBF solution. Hence, to evaluate the changes occurred in electrochemical nature during the apatite formation, the UT, AHT, and AHHT Ti and Ti-5Al-2Nb-1Ta alloy were subjected to potentiodynamic polarization and EIS studies.

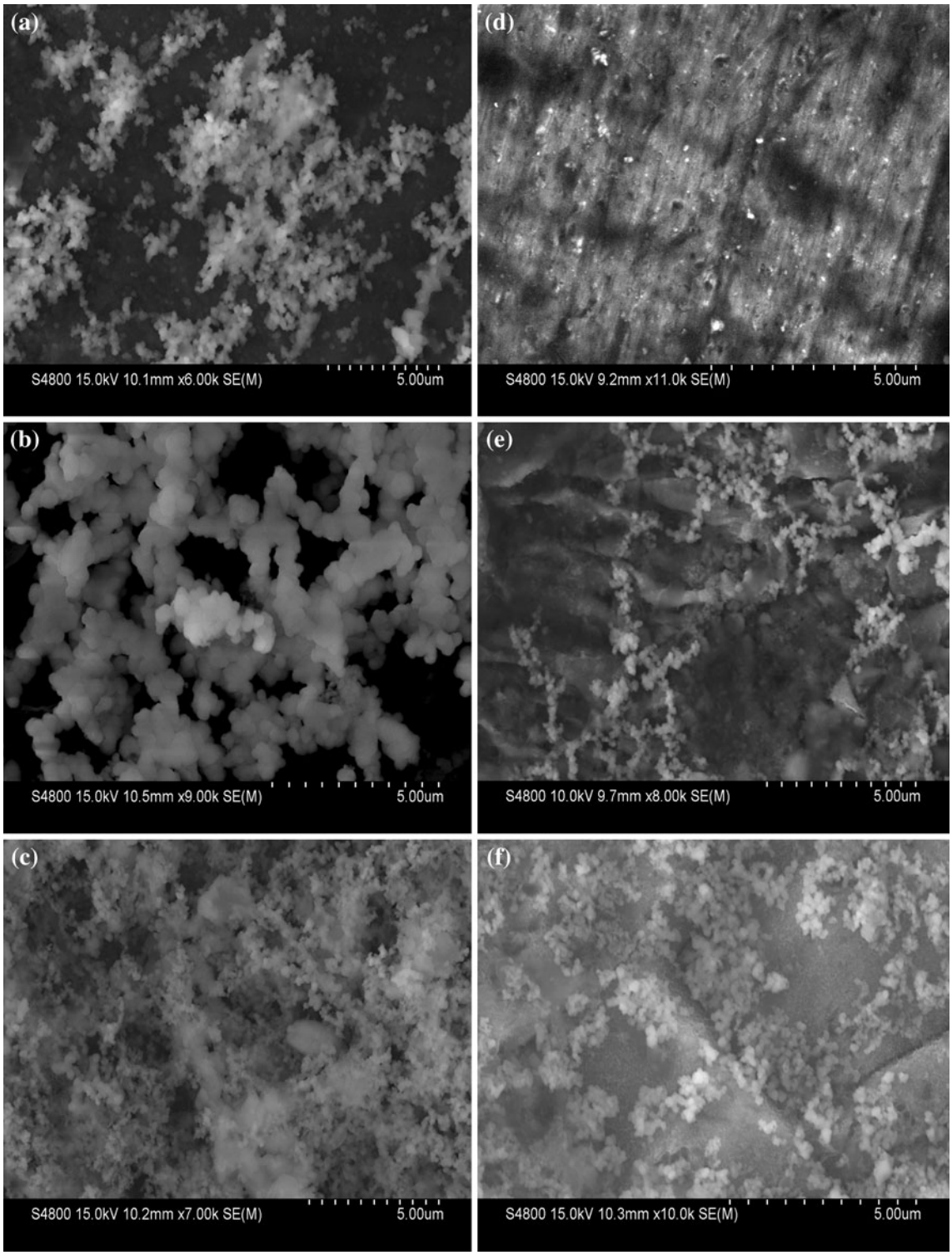

Fig. 6 SEM micrographs of Ti: (a) UT, (b) AHT and (c) AHHT and Ti-5Al-2Nb-1Ta: (d) UT, (e) AHT and (f) AHHT after 7 days of immersion in SBF solution

3.3.1 Potentiodynamic Polarization Studies. The potentiodynamic polarization curves for UT, AHT, and AHHT Ti and Ti-5Al-2Nb-1Ta alloy on immersion in SBF solution are presented in Fig. 7(a) and (b). The polarization behaviors of AHT and AHHT Ti specimens were appreciably different from that of the UT Ti indicating that the chemical and heat treatments produce an effect on the corrosion behavior. The UT Ti exhibited a constant current density value extended over a wide range of potentials immediately after the immersion in the SBF solution. The anodic current at 1.6 V refers to the oxygen evolution process which takes place via electron transfer across the oxide without transpassive dissolution of Ti, whereas the UT Ti-5Al-2Nb-1Ta alloy showed a stable passive film at a potential region of 0.1-1 V. At this region, the current density

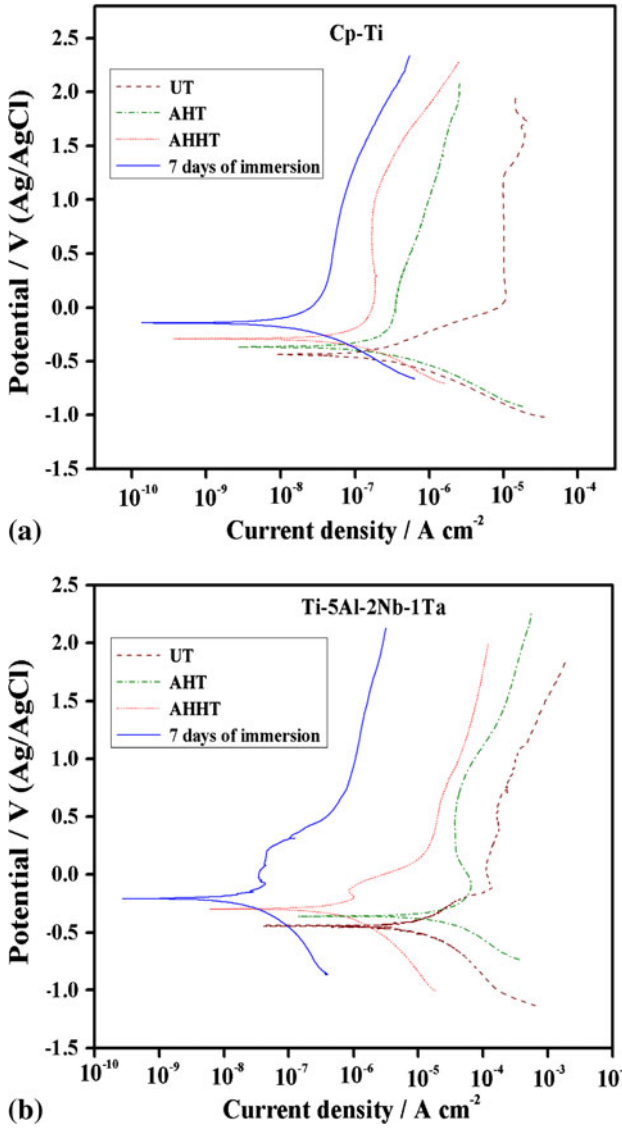

Fig. 7 Potentiodynamic polarization curves of (a) Ti and (b) Ti-5Al-2Nb-1Ta alloy

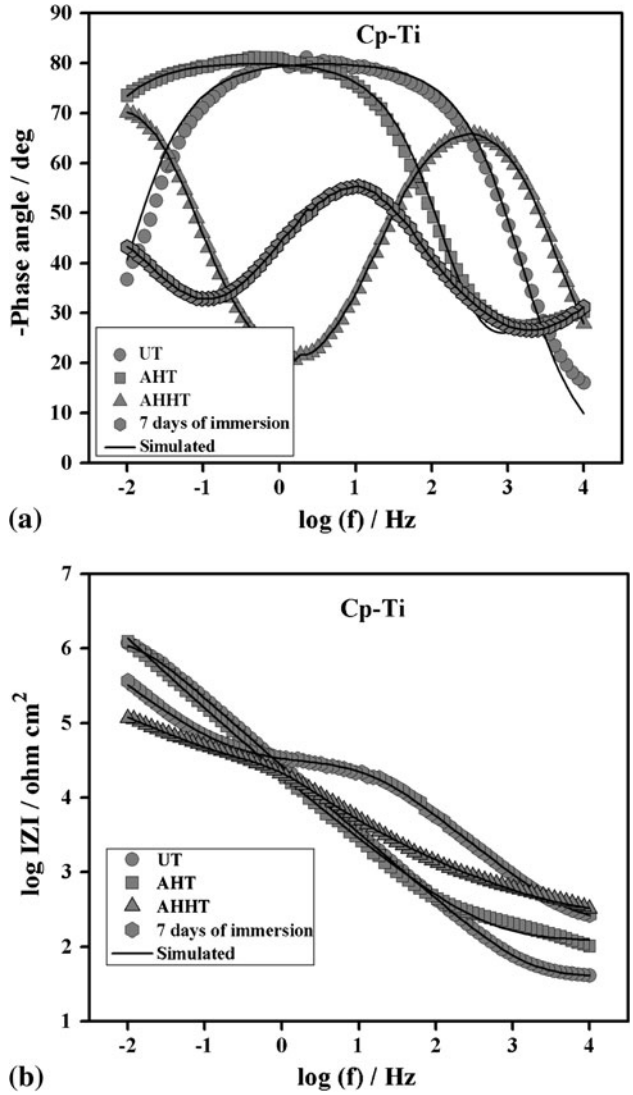

Fig. 8 Bode phase angle (a) and Bode resistance (b) plot of UT, AHT, and AHHT Ti and after 7 days of immersion in SBF solution

remains almost constant indicating the thickening of the anodic surface film (Ref 17). The rapid increase in the anodic current after 1 V refers to the breakdown of the passive film. The AHT Ti showed a steady increase in the current density at the anodic region till 2 V which can be attributed to the thinning of the porous layer formed during the chemical treatment, whereas the AHHT Ti and AHT Ti-5Al-2Nb-1Ta alloy showed a stable current density that remained till 1 V. Beyond 1 V, there is a slight increase in the anodic current density, which may be due to the breakdown of the titanate layer in SBF solution, and a rapid increase in the current density after 0.5 V, representing the dissolution and break down of the gel layer in the SBF solution, was observed for the AHHT Ti-5Al-2Nb-1Ta alloy.

To study the effect of higher immersion time on corrosion resistance of the Ti and Ti-5Al-2Nb-1Ta alloy in SBF solution, potentiodynamic polarization measurements were carried out after 7 days of immersion in SBF solution. Hence, a significant potential shift in the positive direction and a reduction in current density by one order of magnitude were observed for the AHHT Ti and the AHHT Ti-5Al-2Nb-1Ta alloy. This may be due to the incorporation of calcium and phosphate ions present in the SBF solution over the densified gel layer with the surface film formed on Ti-5Al-2Nb-1Ta alloy. Assis et al. (Ref 34) have examined the electrochemical behavior of Ti-6Al-4V and Ti-6Al-7Nb alloys, along with Ti-13Nb-13Zr alloy, and its corrosion resistance in an artificial physiological solution. The results showed that very low current densities were obtained from the polarization curves, indicating a typical passive behavior for the investigated alloys. Hodgson et al. (Ref 35) have reported that the calcium and phosphate ions present in the SBF solution interact with the surface film of Ti alloy and changed the surface properties, which can be attributed to changes in the surface nature of the specimens.

3.3.2 Electrochemical Impedance Spectroscopic Studies. The EIS measurements were carried out for the UT, AHT, and AHHT Ti and Ti-5Al-2Nb-1Ta alloy on immersion in SBF solution, and the Bode plots are presented in Fig. 8(a), (b) and 9(a), (b). The UT Ti and Ti-5Al-2Nb-1Ta alloy showed phase angle values around −80° and −70°, respectively, which remained almost constant over a wide range of frequency regions. This behavior confirmed the formation of passive

oxide film over the Ti surface which is highly insulative and protective against aggressive ion ingression (Ref 16, 19). The AHT Ti and Ti-5Al-2Nb-1Ta alloy showed phase angle values of −15° and −10°, respectively, at the higher frequency, then it shifts to −80° at the intermediate frequency, and approaches to −75° in the lower frequency region. This phase angle shift confirmed the presence of inner barriers and outer porous layers in the higher and lower frequency regions, respectively.

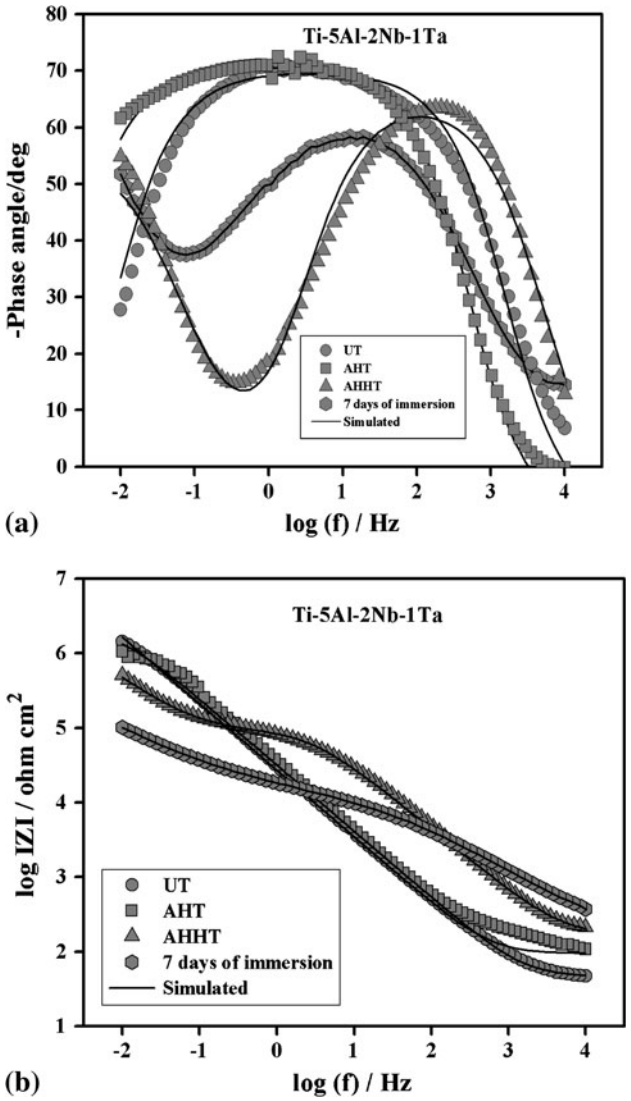

Fig. 9 Bode phase angle (a) and Bode resistance (b) plot of UT, AHT, and AHHT Ti-5Al-2Nb-1Ta alloy and after 7 days of immersion in SBF solution

The AHHT Ti and Ti-5Al-2Nb-1Ta alloy showed two time constants and well-separated range in the frequency domain, and the phase angle approaches to around −60° and −70° in the intermediate frequency region, which corresponds to the formation of passive film over the metal surface, and the secondary region starts at the intermediate frequency and attained phase angle values of −70° and −65° in the lower frequency region. This behavior can be attributed to the formation of a new layer apart from the barrier layer. The formation of a new layer may be the densified gel layer due to the mixture of alkali and hydrogen peroxide followed by heat treatment over the metal surface. The impedance plot showed that there were no significant changes observed for UT and AHT specimens. However, the AHHT Ti and Ti-5Al-2Nb-1Ta specimens exhibited higher resistance values compared to the UT and AHT specimens.

The AHHT Ti and Ti-5Al-2Nb-1Ta alloy after 7 days of immersion in SBF solution showed a slight variation in the phase angle and starts at −35° and −15° in the higher frequency region and approaches to around −55° and −60° at the intermediate frequency, and a small hump at −45° at the lower frequency region, respectively. This indicated the presence of three time constant behavior with inner barrier layer, outer porous layer, and formation of a new layer over the metal surface. However, the AHHT Ti-5Al-2Nb-1Ta alloy exhibited two time constant behavior with inner barrier layer and apatite layer. The formation of a new layer is characteristic of a shift in the phase angle at the lower frequency region. The shift in the phase angle can be attributed to the growth of apatite over the surface-modified Ti and Ti-5Al-2Nb-1Ta alloy. The interaction of solution with the metal surface is generally identified by a phase shift at the higher frequency region which can be attributed to a physical change in the porous layer (Ref 35). It can also be observed that, the solution resistance is high for AHHT Ti-5Al-2Nb-1Ta when compared with AHHT Ti from the calculated values (Table 3), which indicated the adsorption of solution ions over the metal surface. This suggested the repair of the defects in the barrier layer during the period of immersion might have occurred by the incorporation of mineral ions from the solution into the defects/pores or to the film-thickening process during the immersion time (Ref 20, 36).

Table 3 Impedance parameters of Ti and Ti-5Al-2Nb-1Ta alloy obtained by fitting R_s (R_bQ_b), R_s (R_gQ_g) (R_bQ_b), R_s (R_aQ_a) (R_gQ_g) (R_bQ_b) and R_s (R_aQ_a) (R_bQ_b) models on immersion in SBF solution

	R_s, Ω cm^2	R_a, KΩ cm^2	Q_a, μF/cm^2	n	R_g, KΩ cm^2	Q_g, μF/cm^2	n	R_b, KΩ cm^2	Q_b, μF/cm^2	n
Titanium										
UT	42	…	…	…	…	…	…	1684	0.48	0.89
AHT	68	…	…	…	1063	1.93	0.83	2105	18.53	0.90
AHHT	103	…	…	…	2885	2.66	0.76	2924	11.95	0.84
7 days	121	7390	0.26	0.84	1780	1.87	0.82	5978	7.80	0.96
Ti-5Al-2Nb-1Ta										
UT	46	…	…	…	…	…	…	4380	3.08	0.88
AHT	102	…	…	…	1520	14.54	0.79	5983	2.89	0.84
AHHT	159	…	…	…	1869	18.60	0.76	7897	10.02	0.85
7 days	210	6624	6.32	0.87	…	…	…	6580	13.94	0.87

The obtained impedance spectra for UT, AHT, and AHHT Ti and Ti-5Al-2Nb-1Ta alloy on immersion in the SBF solution was fitted using the equivalent circuits which are shown in Fig. 10(a) and (b). The spectra obtained for UT Ti and Ti-5Al-2Nb-1Ta alloy were fitted using an equivalent circuit model represented as R_s (R_bQ_b), where R_s represents the solution resistance, and R_b and Q_b represent the resistance and capacitance of the barrier layer, respectively. It represents the presence of a single layer due to the passive oxide formation over the metal surface (Ref 37). The spectra obtained for AHT and AHHT Ti specimens and Ti-5Al-2Nb-1Ta alloy were fitted using an equivalent circuit model represented as R_s (R_gQ_g) (R_bQ_b) where R_g and Q_g represent the resistance and capacitance of the gel layer, respectively. Wang et al. (Ref 38) proposed similar type of equivalent circuit model to simulate the data for alkali-treated titanium in SBF solution.

The equivalent circuit consisting of three parallel combinations of resistor and capacitor in series with solution resistance is used to fit the spectra obtained for AHHT Ti after 7 days of immersion in SBF solution which are presented in Fig. 10(c). The equivalent circuit model is represented as R_s (R_aQ_a) (R_gQ_g) (R_bQ_b) where, R_a and Q_a represent the charge transfer resistance and double layer capacitance of the apatite layer, respectively. The fitted spectra exhibited the presence of three time constants, indicating the formation of a new layer which may be due to the adsorption of Ca and P ions over the gel layer. The equivalent circuit used to fit the spectra for AHHT Ti-5Al-2Nb-1Ta alloy after 7 days of immersion in SBF solution is shown in Fig. 10(d). The model is represented as R_s (R_aQ_a) (R_bQ_b), where, R_a and Q_a represent the charge transfer resistance and double layer capacitance of the apatite layer, respectively. It represents the two time constant behavior, corresponding to the barrier layer and apatite layer formation. This is due to the adsorption of Ca and P ions over the barrier layer.

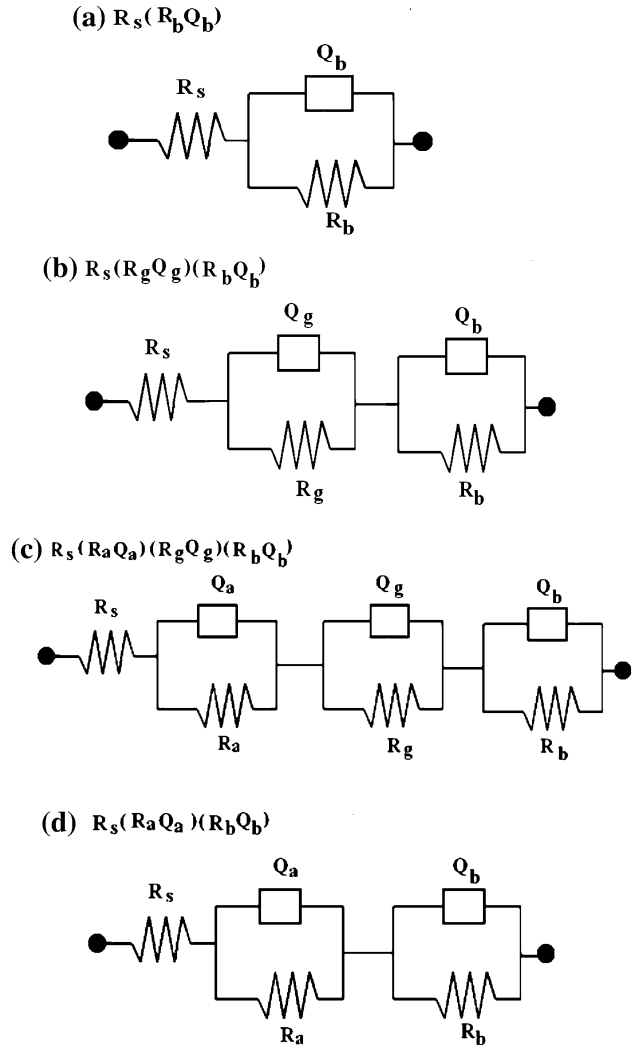

Fig. 10 Equivalent circuit diagrams of Ti and Ti-5Al-2Nb-1Ta alloy (a) UT, (b) AHT, (c) AHHT Ti, and (d) AHHT Ti-5Al-2Nb-1Ta alloy after 7 days of immersion in SBF solution

Thus, the mixture of alkali and hydrogen peroxide induces the formation of a hydrated oxide layer and drives a thickening and roughening of the surface layer. Hence, it can be concluded that, this thicker hydrated oxide layer provides an environment which strongly promotes the calcium phosphate formation and high corrosion resistance over the surface of Ti and Ti-5Al-2Nb-1Ta alloy. Hence, the excellent in vitro bioactivity and high corrosion resistance achieved for AHHT Ti suggest that the surface-modification approach is a viable way of providing Ti implants with desired bioactivity and for achieving an early and stable fixation of Ti implants.

4. Conclusions

To enhance the biocompatibility and corrosion resistance, the surface modifications of Cp-Ti and Ti-5Al-2Nb-1Ta alloy were performed using mixture of alkali and hydrogen peroxide followed by subsequent heat treatment. The surface morphological studies confirmed that the AHT and AHHT Ti specimens exhibited well-defined porous network layers with densified structure. In vitro characterization revealed the formation of apatite layer over the entire surface of AHT and AHHT Ti specimens and randomly scattered over the AHT and AHHT Ti-5Al-2Nb-1Ta specimens. The XRD patterns showed the anatase structure and apatite formation over the surface-modified Ti and Ti-5Al-2Nb-1Ta alloy. The potentiodynamic polarization studies proved that the AHHT Ti after 7 days of immersion in SBF solution exhibited lower current density compared with AHHT Ti-5Al-2Nb-1Ta alloy. The EIS results indicated the appearance of duplex layer for the immediate immersion and exhibited triplex layer after 7 days of immersion in SBF solution for the AHHT Ti. The AHHT Ti-5Al-2Nb-1Ta alloy exhibited a duplex layer formation for immediate and after 7 days of immersion in SBF solution. Hence, the AHHT Ti enhances the biocompatibility and induces the apatite-forming ability within a short period of time compared with the AHHT Ti-5Al-2Nb-1Ta alloy.

Acknowledgment

One of the authors, Y. Sasikumar, acknowledges the financial support received from the Council of Scientific and Industrial Research (CSIR), New Delhi.

References

1. C. Sitting, M. Textor, N.D. Spencer, M. Wieland, and P.H. Vallotton, Surface Characterization, *J. Mater. Sci. Mater. Med.*, 1999, **10**, p 35–46
2. M. Niinomi, D. Kuroda, K. Fukunaga, M. Morinaga, Y. Kato, T. Yashiro, and A. Suzuki, Corrosion Wear Fracture of New Beta Type Biomedical Ti Alloys, *Mater. Sci. Eng. A*, 1999, **263**, p 193–199

3. Y. Okazaki, Effect of Friction on Anodic Polarization Properties of Metallic Biomaterials, *Biomaterials*, 2002, **23**, p 2071–2077
4. M.A. Khan, R.L. Williams, and D.F. Williams, Conjoint Corrosion and Wear in Ti Alloys, *Biomaterials*, 1999, **20**, p 765–772
5. M.A. Khan, R.L. Williams, and D.F. Williams, In Vitro Corrosion and Wear in Ti Alloys in Biological Environments, *Biomaterials*, 1996, **17**, p 2117–2126
6. M.A. Khan, R.L. Williams, and D.F. Williams, The Corrosion Behavior of Ti-6Al-4V, Ti-6Al-7Nb and Ti-13Nb-13Zr in Protein Solutions, *Biomaterials*, 1999, **20**, p 631–637
7. M.F. Semlitsch, H. Weber, R.M. Streicher, and R. Schon, Joint Replacement Components Made of Hot-Forged and Surface-Treated Ti-6Al-7Nb Alloy, *Biomaterials*, 1992, **13**, p 781–788
8. K. Wang, The Use of Ti for Medical Applications in the USA, *Mater. Sci. Eng. A*, 1996, **213**, p 134–137
9. M. Niinomi, Mechanical Properties of Biomedical Ti Alloys, *Mater. Sci. Eng. A*, 1998, **243**, p 231–236
10. R.G. Vardiman and R.A. Kent, Improvement of Fatigue Life of Ti-6Al-4V by Ion Implantation, *J. Appl. Phys.*, 1982, **53**, p 690–694
11. J. Hongbing, L. Xia, M. Xinxin, and Y. Sun, Tribological Performance of Ti-6Al-4V Plasma Based Ion Implanted with Nitrogen, *Wear*, 2000, **246**, p 40–45
12. K.T. Rie and Th. Lampe, Proceedings of the International Conference on Surface Modification of Metals by Ion Beams, *Mater. Sci. Eng.*, 1985, **69**, p 473–481
13. C. Ohtsuki, H. Iida, S. Hayakawa, and A. Osaka, Bioactivity of Ti Treated with Hydrogen Peroxide Solutions Containing Metal Chlorides, *J. Biomed. Mater. Res.*, 1997, **35**, p 39–47
14. H.B. Wen, J.G. Wolke, J.R. Wijn, Q. Liu, F.Z. Cui, and K. de Groot, Fast Precipitation of Calcium Phosphate Layers on Ti Induced by Simple Chemical Treatments, *Biomaterials*, 1997, **18**, p 1471–1478
15. T. Kokubo, F. Miyaji, and H.M. Kim, Spontaneous Formation of Bone Like Apatite Layer on Chemically Treated Ti Metals, *J. Am. Ceram. Soc.*, 1996, **4**, p 1127–1129
16. Y. Sasikumar, M. Karthega, and N. Rajendran, In Vitro Bioactivity of Surface-Modified β-Ti Alloy for Biomedical Applications, *J. Mater. Eng. Perform.*, 2011, **20**, p 1271–1277
17. S. Tamilselvi and N. Rajendran, In Vitro Corrosion Behavior of Ti-5Al-2Nb-1Ta Alloy in Hanks Solution, *Mater. Corros.*, 2007, **58**, p 285–289
18. S. Tamilselvi, V. Raman, and N. Rajendran, Evaluation of Corrosion Behavior of Surface-Modified Ti-6Al-4V ELI, Alloy in Hanks Solution, *J. Appl. Electrochem.*, 2010, **40**(2), p 285–293
19. S. Tamilselvi, V. Raman, and N. Rajendran, Surface Modification of Ti by Chemical and Thermal Methods—Electrochemical Impedance Spectroscopic Studies, *Corros. Eng. Sci. Technol.*, 2010, doi:10.1179/147842209X12590591256936
20. M. Karthega, S. Nagarajan, and N. Rajendran, In Vitro Studies of Hydrogen Peroxide Treated Ti for Biomedical Applications, *Electrochim. Acta*, 2010, **55**, p 2201–2209
21. T. Kokubo and H. Takadama, How Useful is SBF in Predicting In Vivo Bone Bioactivity, *Biomaterials*, 2005, **27**, p 2907–2915
22. Y. Zhou, Y.B. Wang, E.W. Zhang, Y. Cheng, X.L. Xiong, Y.F. Zheng, and S.C. Wei, Alkali Heat Treatment of a Low Modulus Biomedical Ti-27Nb Alloy, *Biomed. Mater.*, 2009, **4**, p 044108–044111
23. J.-H. Yi, C. Bernard, F. Variola, S.F. Zalzal, J.D. Wuest, F. Rosei, and A. Nanci, Characterization of a Bioactive Nanotextured Surface Created by Controlled Chemical Oxidation of Titanium, *Surf. Sci.*, 2006, **600**, p 4613–4621
24. N. Chosa, M. Taira, S. Saitoh, N. Sato, and Y. Araki, Characterization of Apatite Formed on Alkaline Heat-Treated Ti, *J. Dent. Res.*, 2004, **83**, p 465–469
25. T. Lindgren, J.H. Muabora, E. Avendeno, J. Jonsson, A. Hoel, C.G. Granquist, and S.E. Lindquist, Photo Electrochemical and Optical Properties of Nitrogen Doped Ti Dioxide Films Prepared by Reactive DC Magnetron Sputtering, *J. Phys. Chem. B*, 2003, **107**, p 5709–5716
26. L.L. Hench, Medical Materials for the Next Millennium, *Mater. Res. Soc.*, 1999, **24**, p 13–19
27. T. Kokubo, H. Kushitani, S. Sakka, T. Kitsugi, and T. Yamamuro, Solutions Able to Reproduce In-Vivo Surface Structure Changes in Bioactive Glass-Ceramics, *J. Biomed. Mater. Res.*, 1990, **24**, p 721–734
28. S. Koutsopoulos, Synthesis and Characterization of Hydroxyapatite Crystals: A Review Study on the Analytical Methods, *J. Biomed. Mater. Res.*, 2002, **62**, p 600–612
29. F. Liang, L. Zhou, and K. Wang, Apatite Formation on Porous Ti by Alkali and Heat-Treatment, *Surf. Coat. Technol.*, 2003, **165**, p 133–139
30. F. Liang, L. Zhou, and K. Wang, Enhancement of the Bioactivity of Alkali-Heat Treated Ti by Pre-Calcification, *J. Mater. Sci. Lett.*, 2003, **22**, p 1665–1669
31. F.H. Lin, Y.S. Hsu, S.H. Lin, and T.M. Chen, The Growth of Hydroxyapatite on Alkaline Treated Ti-6Al-4V Soaking in Higher Temperature with Concentrated Ca^{2+}/HPO_4^{2-} Simulated Body Fluid, *Mater. Chem. Phys.*, 2004, **87**, p 24–30
32. H. Takadama, H.M. Kim, T. Kokubo, and T. Nakamura, An X-Ray Photoelectron Spectroscopy Study of the Process of Apatite Formation on Bioactive Ti Metal, *J. Biomed. Mater. Res.*, 2001, **55**, p 185–193
33. P. Shi, F. Geng, and F.T. Cheng, Preparation of Titania-Hydroxyapatite Coating on NiTi via a Low Temperature Route, *Mater. Lett.*, 2006, **60**, p 1996–1999
34. S. Assis, S. Wolynee, and I. Costa, Corrosion Characterization of Ti Alloys by Electrochemical Techniques, *Electrochim. Acta*, 2006, **51**, p 1815–1819
35. A.W.E. Hodgson, Y. Mueller, D. Forster, and S. Virtanen, *Electrochim. Acta*, 2002, **47**, p 1913–1923
36. A.K. Shukla and R. Balasubramaniam, Effect of Surface Treatment on Electrochemical Behaviour of Cp-Ti, Ti-6Al-4V and Ti-13Nb-13Zr Alloys in Simulated Human Body Fluid, *Corros. Sci.*, 2005, **48**, p 1696–1720
37. J.E.G. Gonzalez and J.C. Mirza Rosca, Study of the Corrosion Behavior of Ti and Its Alloys for Biomedical and Dental Implant Applications, *J. Electroanal. Chem.*, 1999, **471**, p 109–115
38. C.X. Wang, M. Wang, and X. Zhou, Electrochemical Impedance Spectroscopy Study of the Nucleation and Growth of Apatite on Chemically Treated Ti, *Langmuir*, 2002, **18**, p 7641–7647